

*Montmorillonite incorporated
polymethylmethacrylate matrix containing
lithium trifluoromethanesulphonate
(LTF) salt: thermally stable polymer
nanocomposite electrolyte for lithium-ion
batteries application*

Emad M. Masoud

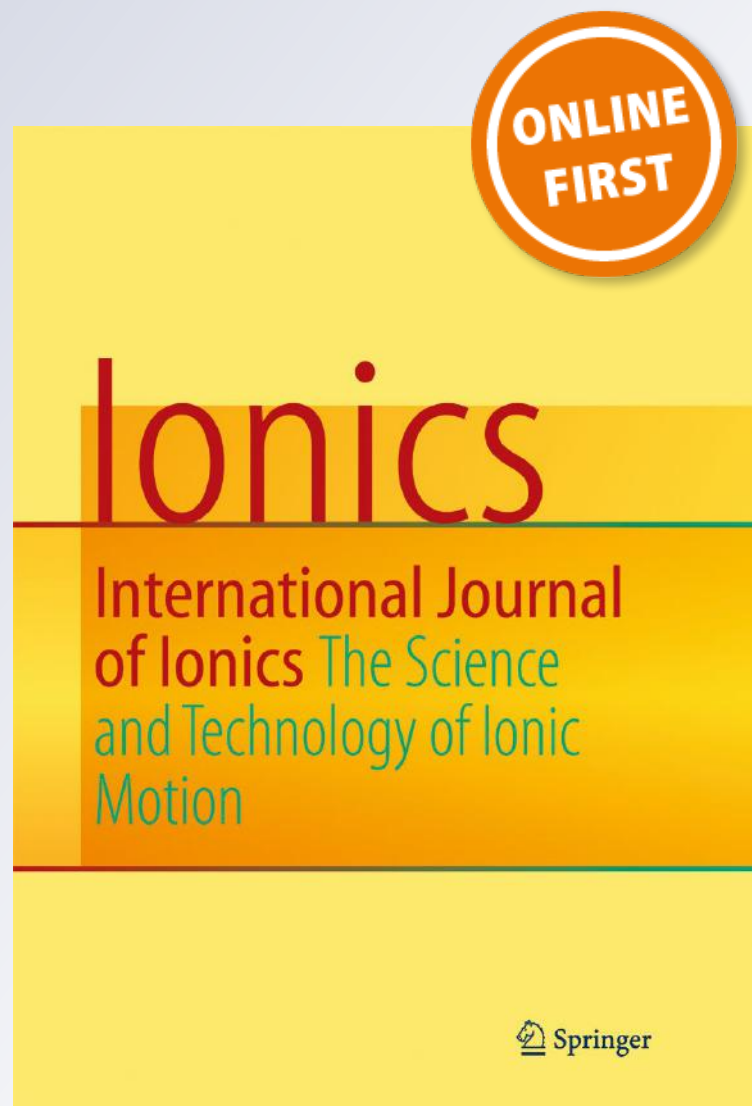
Ionics

International Journal of Ionics The
Science and Technology of Ionic Motion

ISSN 0947-7047

Ionics

DOI 10.1007/s11581-018-2802-1



Your article is protected by copyright and all rights are held exclusively by Springer-Verlag GmbH Germany, part of Springer Nature. This e-offprint is for personal use only and shall not be self-archived in electronic repositories. If you wish to self-archive your article, please use the accepted manuscript version for posting on your own website. You may further deposit the accepted manuscript version in any repository, provided it is only made publicly available 12 months after official publication or later and provided acknowledgement is given to the original source of publication and a link is inserted to the published article on Springer's website. The link must be accompanied by the following text: "The final publication is available at link.springer.com".



Montmorillonite incorporated polymethylmethacrylate matrix containing lithium trifluoromethanesulphonate (LTF) salt: thermally stable polymer nanocomposite electrolyte for lithium-ion batteries application

Emad M. Masoud¹

Received: 19 August 2018 / Revised: 1 November 2018 / Accepted: 12 November 2018

© Springer-Verlag GmbH Germany, part of Springer Nature 2018

Abstract

High and low content of montmorillonite incorporated polymethylmethacrylate matrix in the presence of lithiumtriflate salt was investigated and studied. All samples were synthesized using the solution cast technique method. Different techniques (X-ray diffraction, FT-IR, DSC, TG, and SEM) were used for structure characterization. X-ray diffraction (XRD) and Fourier transform infrared (FT-IR) analyses confirmed the complete dissolution of lithiumtriflate salt and intercalation of montmorillonite within the polymethylmethacrylate matrix. The different contents of montmorillonite showed different behaviors in both of structure and properties. The sample containing the low content of 5 wt% montmorillonite showed the highest AC- conductivity value ($\sigma_{AC} = 2.09 \times 10^{-6} \Omega^{-1} \cdot \text{cm}^{-1}$, at room temperature) with a big difference to the other ones. The same sample also showed a good thermal stability ($T_d = 378 \text{ }^\circ\text{C}$). Electrochemical stability of the same sample was also studied. All results were collected and discussed.

Keywords Montmorillonite · Electrical properties · Polymer nanocomposites electrolytes · Electrochemical stability · Lithium ion batteries

Introduction

Solid electrolytes have received attention as electrolytic materials for solid lithium-ion batteries because of advantages in mechanical stability, safety, flexibility, and processability. The solid polymer electrolytes are flexible-type solid-state ion-dipolar complexes recognized as the most suitable ion-conducting dielectric materials for the development

of dry-state high energy density rechargeable batteries [1–8]. Polymers such as poly(vinylidene fluoride) (PVdF) [9] and its co-polymer poly(vinylidene fluoride-co-hexafluoro propylene) P(VdF-co-HFP) [10, 11], poly(methyl methacrylate) (PMMA) [12], poly(acrylonitrile) (PAN) [13], polyethylene oxide PEO [14–16], and its blends [17] have been widely studied as host polymers for preparing polymer electrolytes. PMMA is one of the promising representatives of polymeric materials with a wide application, especially as electrolytes for lithium-ion batteries. To date, it has to satisfy various constraints in regard to amorphous nature, stability against degradation, limits on charge traps, high breakdown potential, band offsets processability, and reproducibility [18]. Extensive work has been performed to tune the properties such as morphology, optical, dielectric, and aging behavior of PMMA films. Till now, the better outcomes were gotten from ionogel with the marvelous compatibility of different organic salts with PMMA [19–22]. The enhancement effect of various ceramic particles, like SiO₂, TiO₂, ZnO, Al₂O₃, etc., on the conductivities and electrochemical stability of polymer electrolytes was also well documented in the literature [23–25]. The addition of fillers with Lewis acids surface groups usually reduces the

Highlights • High and low MMT contents incorporated PMMA matrix containing LTF salt were investigated and studied.

- Different structures and properties were observed in the presence of MMT content.
- The low MMT content (5 wt% montmorillonite) within the PMMA matrix showed the best suitable matrix for the lithium-ion diffusion.
- The same sample showed the highest conductivity value, with a big difference to the others.
- Good thermal and electrochemical stability behavior was also observed.

✉ Emad M. Masoud
emad.youssef@fsc.bu.edu.eg; emad_masoud1981@yahoo.com;
<http://www.bu.edu.eg/staff/emadyoussef7>

¹ Chemistry Department, Faculty of science, Benha University, Benha 13518, Egypt

ion pairing and therefore increases the conductivity. On the other hand, stabilization of the interphase and lowering of the overall resistance of lithium electrodes was observed when using surface-modified inorganic fillers as additives [26–28]. Although not widely studied as ceramic powders, montmorillonite clay is another type of inorganic filler that enhanced the conductivity of PEO [29–32] and poly-(acrylonitrile) (PAN) [33]. This enhancement was due to the well-dispersed clay in the system, which tended to disrupt the association of lithium cations and anions [31]. Many research works investigated the clay–PMMA composites as gel electrolytes and only in the low contents [34, 35]. Many researchers present encouraging results for P (VdF-HFP)-based polymer electrolytes with different types of dopant salts, such as lithium fluoroalkyl phosphate [36], lithium perchlorate [37], and lithium bis(trifluoromethanesulfonyl) imide [38]. Lithium trifluoromethanesulfonate salt (LTFMS) is one of the most common lithium salts used in polymer electrolyte research. Here, and as a continuation of our previous works concerning the polymer electrolytes, a new trial of using the nanomontmorillonite clay as filler will be studied and conducted in both low and high contents, into polymethylmethacrylate matrix containing lithiumtriflate salt. These nanocomposites will be studied as solid electrolytes for achieving the two main properties: ionic conductivity and thermal stability.

Experimental

Synthesis of pure polymer, polymer electrolyte, and polymer nanocomposite electrolytes

Materials: PMMA (polymethylmethacrylate, M.wt = 300,000, Sigma-Aldrich, 99.99%), LiCF_3SO_3 (lithium trifluoromethane sulphonate, Sigma-Aldrich, 99.99%), DMF (N, N Di-methyl formamide, Sigma-Aldrich, 99.99%), and montmorillonite (nanoclay, specific surface area = 240 m^2/g , Sigma-Aldrich, 99.99%).

Pure polymer, polymer electrolyte and polymer nanocomposite electrolytes were prepared using a simple solution casting technique. PMMA was first dissolved in N, N Di-methyl formamide (DMF) under heating (40 °C) till a homogeneous viscous solution is obtained. After that, LiCF_3SO_3 salt was added. Following, different montmorillonite (nano clay) filler amounts were added to the viscous solution according to the following concentration formula:

$$[90 \text{ PMMA} - 10 \text{ LiCF}_3\text{SO}_3]_{100-x} + x \text{ Montmorillonite (nano clay)}, x = 0, 5, 10, 30, 50 \text{ wt\%}$$

The solution was continuously stirred for 24 h to avoid the nano filler aggregation and to get the fine mixing. The obtained homogenous viscous solution was then poured into the

petri dish. The solvent was allowed to evaporate slowly from the composite at room temperature and then all samples were dried at 60 °C for 3 h to get pure polymer, polymer electrolyte and polymer nanocomposites electrolytes membranes. All samples were denoted as following: MMT, PMMA, PMMA-LTF, PMMA-LTF-1, PMMA-LTF-2, PMMA-LTF-3, and PMMA-LTF-4 for montmorillonite, pure polymethylmethacrylate, polymethylmethacrylate containing 10 wt% of LiCF_3SO_3 , polymethylmethacrylate containing 10 wt% of LiCF_3SO_3 and 5 wt% montmorillonite (nano clay), polymethylmethacrylate containing 10 wt% of LiCF_3SO_3 and 10 wt% montmorillonite (nano clay), polymethylmethacrylate containing 10 wt% of LiCF_3SO_3 and 30 wt% montmorillonite (nano clay), and polymethylmethacrylate containing 10 wt% of LiCF_3SO_3 and 50 wt% montmorillonite (nano clay), respectively.

Characterization of samples

X-ray diffraction analysis was performed on a Diano (made by Diano Corporation, USA) with Cu-filtered $\text{CuK}\alpha$ radiation ($\lambda = 1.5418 \text{ \AA}$) energized at 45 kV, and 10 mA. The samples were measured at room temperature in the range from $2\theta = 10$ to 70° . Differential scanning calorimetry (DSC) and thermal gravimetric (TG) analyses were performed in air atmosphere, in a temperature range of 303–813 K with a constant heating rate of 10 °C/min using Shimadzu DSC-60H. The Fourier transform infrared spectra of the samples were recorded in the range of 650–4000 cm^{-1} using a Bruker FT-IR. Scanning electron microscopy was carried out with JOEL scanning electron microscope (JSM-35CF). The thickness of each sample was measured using a micrometer screw gauge. Electrical properties were studied in a temperature range from 303 to 373 K and a frequency one from 100 Hz to 10 MHz. Also, these properties were estimated with the help of stainless steel blocking electrodes using a programmable automatic LCR bridge (Model RM 6306 Phillips Bridge).

The electrochemical stability of optimized polymer nanocomposite electrolyte of high ionic conductivity value was evaluated using lithium metal as working and counter electrode, by linear sweep voltammetry at room temperature using an EG&G Electrochemical analyzer (Model-6310) in the scan rate of 1 mV/s.

Results and discussion

X-ray diffraction patterns of LTF, MMT, PMMA, PMMA-LTF, PMMA-LTF-1, PMMA-LTF-2, PMMA-LTF-3, and PMMA-LTF-4 are displayed in Figs. 1 and 2.

Firstly, Fig. 1 showed the effect of LTF addition into the PMMA matrix. The figure showed that the LTF-crystalline peaks completely disappeared in the presence of the

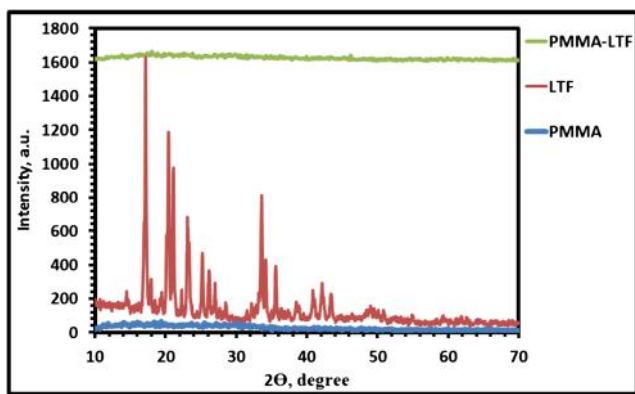


Fig. 1 X-ray diffraction patterns of PMMA, LTF, and PMMA-LTF

amorphous PMMA matrix. This confirms the good interactions between LTF and the polymer matrix, and indicating the good ability of the polymer matrix to dissolve this used concentration of LTF. In contrast, the effect of MMT addition into the PMMA matrix containing LTF salt was also shown (Fig. 2a, b). Figure 2a showed the major amorphosity of all investigated samples containing the different concentrations of MMT. To further show and ensure the interaction nature between MMT and the PMMA matrix containing the LTF salt, X-ray diffraction patterns of the MMT peak (001) (at $2\theta = 4.47$, corresponding to an interlayer spacing of 2 nm) in all PMMA-LTF nanocomposites were introduced in Fig. 2c. The figure showed that this characteristic peak of MMT was shifted to lower 2θ values, corresponding to different interlayer spacing values in the PMMA-LTF nanocomposites. This exhibits the intercalation of PMMA chains inside the galleries of MMT. This intercalation process can be represented through Scheme 1.

As obviously shown, the PMMA-LTF-3 sample showed the lowest 2θ shift value compared to the other ones. This may indicate that this sample has the highest intercalation between both of the PMMA matrix and MMT. Figure 3a shows FT-IR spectra of LTF, MMT, PMMA, PMMA-LTF, PMMA-LTF-1, PMMA-LTF-2, PMMA-LTF-3, and PMMA-LTF-4. Figure 3b shows FT-IR spectra (in a region between 700 and 1700 cm^{-1} , to show obviously the basic bands) of PMMA-LTF-1, PMMA-LTF-2, PMMA-LTF-3, and PMMA-LTF-4. For the basic bands of the PMMA matrix, and according to a literature work [39], it can be seen that there is a distinct absorption band from 1150 to 1250 cm^{-1} , which can be attributed to the C–O–C stretching vibration. The two bands at 1388 and 754 cm^{-1} can be attributed to the α -methyl group vibrations. The band at 987 cm^{-1} is the characteristic absorption vibration of PMMA, together with the bands at 1062 and 843 cm^{-1} . The band at 1732 cm^{-1} shows the presence of the acrylate carboxyl group. The band at 1444 cm^{-1} can be attributed to the bending vibration of the C–H bonds of the $-\text{CH}_3$ group. The two bands at 2997 and 2952 cm^{-1} can be assigned to the C–H bond stretching

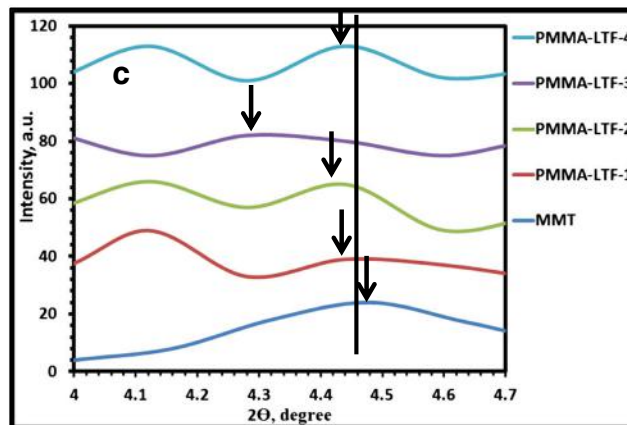
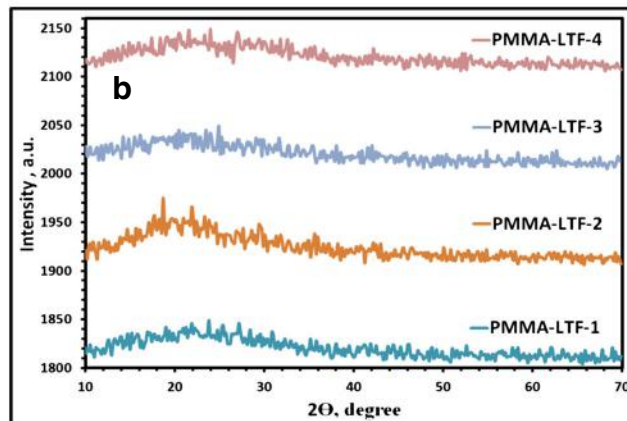
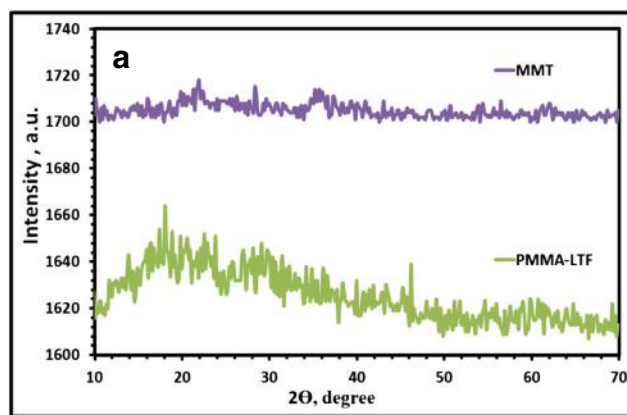
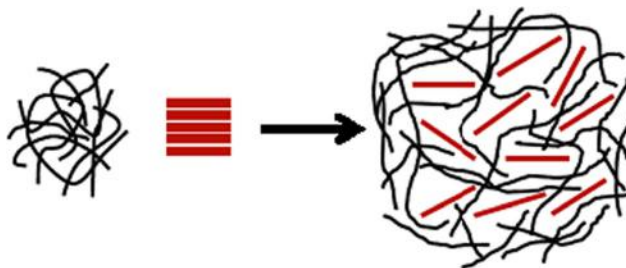


Fig. 2 X-ray diffraction patterns of a PMMA-LTF and MMT; b PMMA-LTF-1, PMMA-LTF-2, PMMA-LTF-3, and PMMA-LTF-4; and c MMT peak (001) in all PMMA-LTF nanocomposites (in a range of $4-4.7^\circ$)



Scheme 1 Intercalation between MMT and the PMMA matrix

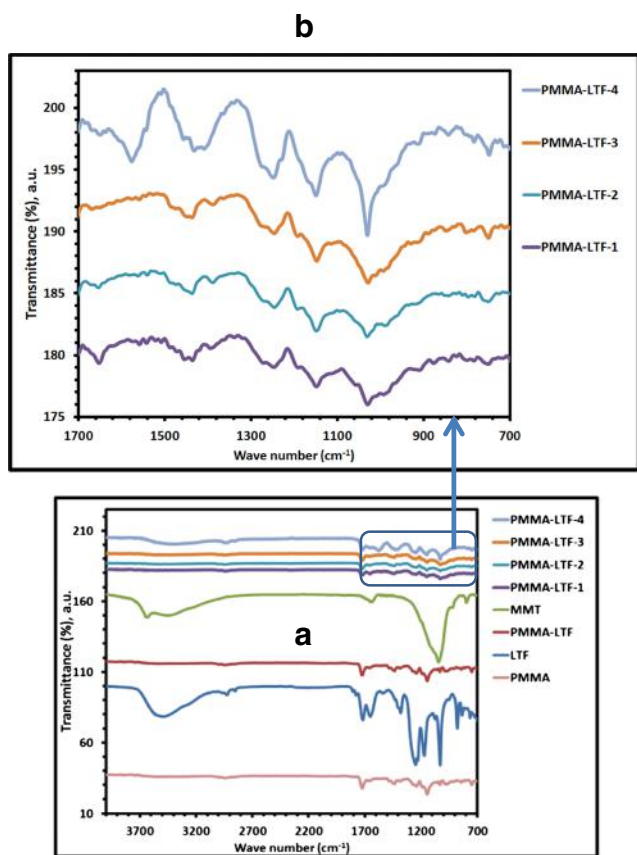


Fig. 3 **a** FT-IR spectra of PMMA, LTF, PMMA-LTF, MMT, PMMA-LTF-1, PMMA-LTF-2, PMMA-LTF-3, and PMMA-LTF-4. **b** FT-IR spectra of PMMA-LTF-1, PMMA-LTF-2, PMMA-LTF-3, and PMMA-LTF-4 in a region of 700–1700 cm^{-1}

vibrations of the $-\text{CH}_3$ and $-\text{CH}_2$ groups, respectively. Furthermore, there are two weak absorption bands at 3437 and 1641 cm^{-1} , which can be attributed to the $-\text{OH}$ group stretching and bending vibrations, respectively. To further investigate the interactions between both of LTF and MMT with the PMMA matrix, a comparison between the wave number values of PMMA bands in both of PMMA-LTF and those of PMMA-LTF containing different concentrations of MMT were collected and tabulated (Table 1). The table showed that there is an observed increase or decrease wave number values shift of PMMA bands in the presence of both LTF and MMT. This increase or decrease shift confirms the interactions between lithium ions of LTF and oxygen – polar group of PMMA, in addition to the above confirmed interactions between MMT and PMMA. DSC thermograms of PMMA, PMMA-LTF, PMMA-LTF-1, PMMA-LTF-2, PMMA-LTF-3, and PMMA-LTF-4 are shown in Fig 4. As obviously shown, the peak observed at a temperature range between 83.5 and $113.2 \text{ }^\circ\text{C}$ for all investigated samples was mainly due to the dehydration process of water molecules. The peak at a temperature range between 133.8 and $163 \text{ }^\circ\text{C}$ can be attributed to the melting temperature (T_m). All melting

Table 1 FT-IR spectral basic bands assignment of PMMA, PMMA-LTF, PMMA-LTF-1, PMMA-LTF-2, PMMA-LTF-3, and PMMA-LTF-4

Wave number (cm^{-1})	PMMA	PMMA-LTF	PMMA-LTF-1	PMMA-LTF-2	PMMA-LTF-3	PMMA-LTF-4
1150–1250	C–O–C stretching vibration	1030–1247	1145–1242	1029–1247	1030–1245	1028–1245
1388, 754	α -Methyl group vibrations	1385, 751	1387, 750	1384, 751	1386, 749	1379, 748
843, 987, 1062	Characteristic absorption vibration of PMMA	840, 983, 1060	841, 987, 1059	838, 985, 1061	842, 984, 1058	845, 985, 1063
1732	Acrylate carboxyl group	1731	1729	1733	1734	1730
1444	Bending vibration of the C–H bonds of the $-\text{CH}_3$ group	1445	1442	1443	1441	1445
2952, 2997	C–H bond stretching vibrations of the $-\text{CH}_3$ and $-\text{CH}_2$ groups	2950, 2995	2954, 2996	2949, 2995	2953, 2989	2948, 2999
1641, 3437	$-\text{OH}$ group stretching and bending vibrations	1640, 3438	1639, 3439	1639, 3434	1643, 3438	1644, 3435

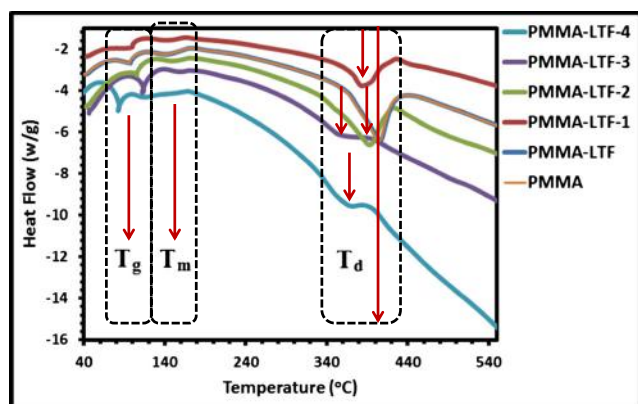


Fig. 4 Differential thermal analysis (DSC) patterns of PMMA, PMMA-LTF, PMMA-LTF-1, PMMA-LTF-2, PMMA-LTF-3, and PMMA-LTF-4

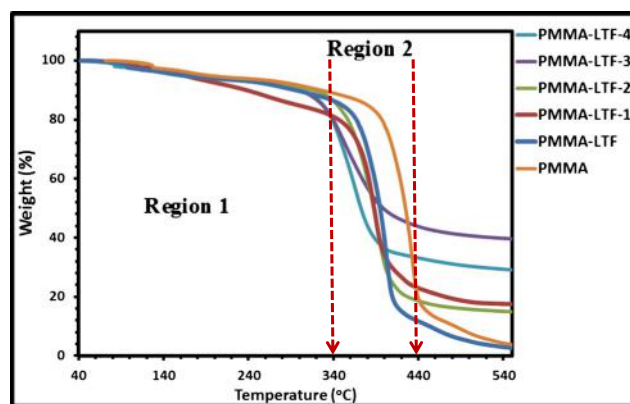


Fig. 5 Thermal gravimetric analysis (TG) patterns of PMMA, PMMA-LTF, PMMA-LTF-1, PMMA-LTF-2, PMMA-LTF-3, and PMMA-LTF-4

temperature values were exactly determined and tabulated (Table 2). Also, the obvious peak at a temperature range between 347 and 438 °C can be attributed to the decomposition temperature (T_d) of the PMMA matrix (Table 2). As is well known, thermal stability property is one of the most important properties determining the ability of the membrane to be used as an electrolyte for lithium ion batteries application. In this vein, investigation of decomposition temperatures (T_d) of all investigated samples was performed through thermal gravimetric analysis, TG, to study the addition effect of both LTF and MMT on the PMMA matrix. Figure 5 revealed two basic weight loss regions; the first was in a temperature range between 40 to 340 °C, and the second one was in a temperature range between 340 to 440 °C. The first region can be attributed to the dehydration of water molecules and melting processes, as confirmed above through the endothermic peaks of the DSC analysis. The second one can also be attributed to the decomposition temperature of the PMMA matrix. This decomposition was also confirmed above through the endothermic peaks of the DSC analysis. According to Table 2 and Fig. 6, the sample containing 30% MMT (PMMA-LTF-3) showed the highest value of melting temperature ($T_m = 163$ °C) compared to the other ones, which showed the following order: (PMMA-LTF-4, $T_m = 142$ °C > PMMA-LTF-2,

$T_m = 140$ °C > PMMA-LTF, $T_m = 135$ °C > PMMA-LTF-1, $T_m = 134$ °C > PMMA, $T_m = 133.8$ °C). In contrast, the pure PMMA sample showed the highest value of decomposition temperature ($T_d = 438$ °C) compared to the other ones, which showed the following order: (PMMA-LTF, $T_d = 408$ °C > PMMA-LTF-2, $T_d = 387$ °C > PMMA-LTF-1, $T_d = 378$ °C > PMMA-LTF-4, $T_d = 364$ °C > PMMA-LTF-3, $T_d = 347$ °C). Here, one can notice that the PMMA-LTF-3 sample of the lowest decomposition temperature (T_d) is the same one of the highest intercalation percent, as confirmed by partially enlarged drawing of MMT peak (001) in all PMMA-LTF nanocomposites (Fig. 2b).

Figure 7 shows the scanning electron microscope analysis in two different magnifications for all investigated samples. All samples revealed the presence of MMT. Furthermore, almost of investigated samples showed the homogeneity distribution of MMT particles within the PMMA matrix, in both of the two magnifications.

The temperature dependence of AC- electrical conductivity of PMMA, PMMA-LTF, PMMA-LTF-1, PMMA-LTF-2, PMMA-LTF-3, and PMMA-LTF-4 was investigated in a temperature range of 303–373 K and at a frequency of 100 Hz

Table 2 Values of melting temperature (T_m), heat enthalpy of melting (ΔH_m), crystallinity percent (X_c), decomposition temperature (T_d), and AC-ionic conductivity (σ_{AC}) of PMMA, PMMA-LTF, PMMA-LTF-1, PMMA-LTF-2, PMMA-LTF-3, and PMMA-LTF-4

Sample	T_m (°C)	T_d (°C)	σ_{AC} (ohm ⁻¹ .cm ⁻¹) at 303 K
PMMA	133.8	438	1.37×10^{-11}
PMMA-LTF	135	408	2.66×10^{-10}
PMMA-LTF-1	134	378	2.09×10^{-6}
PMMA-LTF-2	140	387	3.73×10^{-10}
PMMA-LTF-3	163	347	1.01×10^{-10}
PMMA-LTF-4	142	364	1.48×10^{-10}

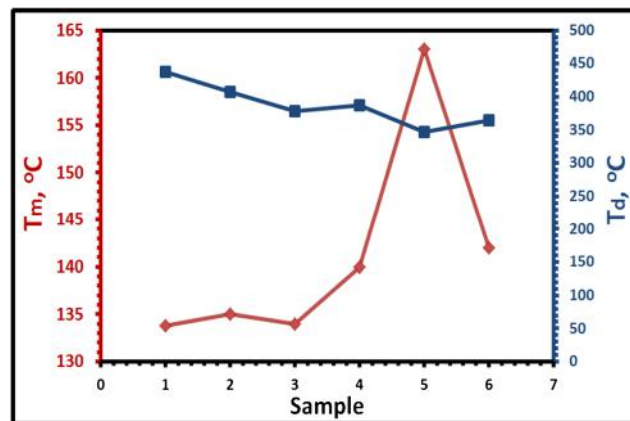
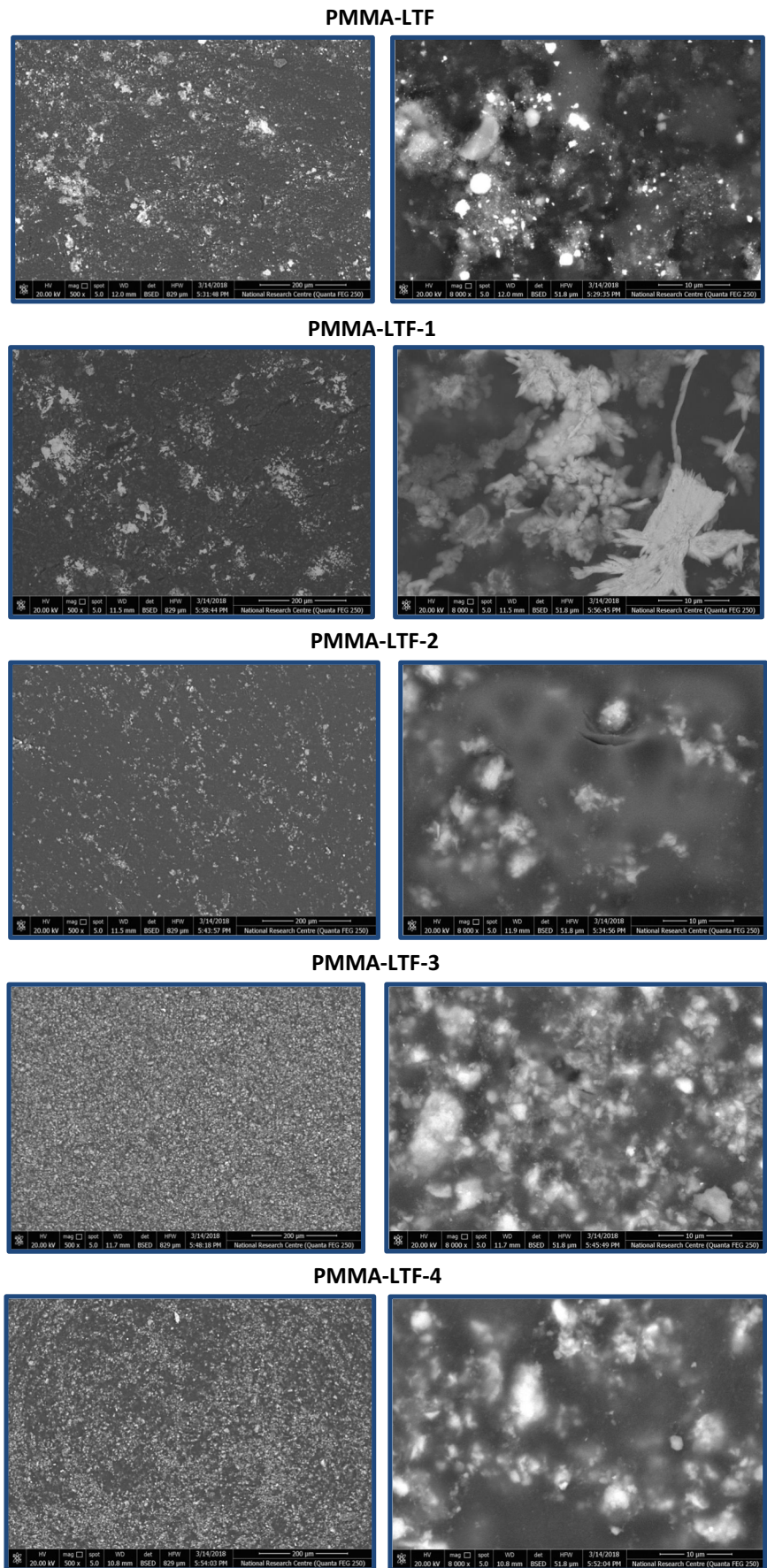


Fig. 6 Melting and decomposition temperatures values for 1: PMMA; 2: PMMA-LTF; 3: PMMA-LTF-1; 4: PMMA-LTF-2; 5: PMMA-LTF-3, and 6: PMMA-LTF-4

Fig. 7 Scanning electron microscope (SEM) photographs of PMMA-LTF, PMMA-LTF-1, PMMA-LTF-2, PMMA-LTF-3, and PMMA-LTF-4



(Fig. 8). In general, the figure revealed that the AC- conductivity increases with temperature increase for all investigated samples. As the conductivity–temperature data follow the Arrhenius behavior, the mechanism of ion transport is deduced to be similar to that in ionic crystals, where ions jump into neighboring vacant sites and thus increase the ionic conductivity to a higher value. The motion of ions in polymer electrolytes is a liquid-like mechanism, by which the movement of ions through the polymer matrix is assisted by the large amplitude of the polymer segmental motion. Thus, greater segmental motion at higher temperatures either permits the ions to hop from one site to another or provides a pathway for ions to move with faster ionic conduction [40]. The PMMA-LTF sample showed higher AC- conductivity value than that of the pure one, PMMA. This shows that the complete dissolution of LTF, confirmed by x-ray diffraction analysis, can induce free mobile lithium ions within the PMMA matrix. On the other hand, the samples of MMT showed different AC- conductivity values. All AC- conductivity values at room temperature were determined (Fig. 9). The figure showed that the AC- conductivity value increased till 5 wt% MMT (PMMA-LTF-1), then a sharp decrease behavior was observed up to 30 wt% (PMMA-LTF-3), then a slight increase was again observed for 50 wt% (PMMA-LTF-4). Table 2 showed that PMMA-LTF-1 sample have the highest AC- conductivity value ($\sigma_{Ac} = 2.09 \times 10^{-6} \Omega^{-1} \cdot \text{cm}^{-1}$, at room temperature) compared to the other ones, which showed the following conductivity order: (σ_{Ac} (PMMA-LTF-2, $3.73 \times 10^{-10} \Omega^{-1} \cdot \text{cm}^{-1}$) > σ_{Ac} (PMMA-LTF, $2.66 \times 10^{-10} \Omega^{-1} \cdot \text{cm}^{-1}$) > σ_{Ac} (PMMA-LTF-4, $1.48 \times 10^{-10} \Omega^{-1} \cdot \text{cm}^{-1}$) > σ_{Ac} (PMMA-LTF-3, $1.01 \times 10^{-10} \Omega^{-1} \cdot \text{cm}^{-1}$) > σ_{Ac} (PMMA, $1.37 \times 10^{-11} \Omega^{-1} \cdot \text{cm}^{-1}$), at room temperature). From these results, we can conclude that the amount of MMT as an inorganic filler within the PMMA matrix play an important role in providing special conducting pathways for the free lithium ions at the filler surface region through Lewis acid base interactions among

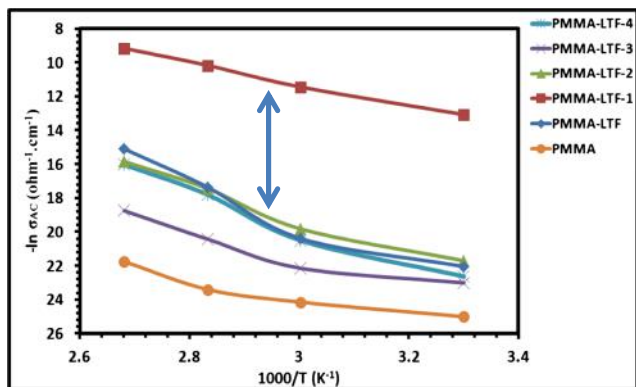


Fig. 8 Temperature dependence of AC- conductivity for PMMA, PMMA-LTF, PMMA-LTF-1, PMMA-LTF-2, PMMA-LTF-3, and PMMA-LTF-4 at a frequency of 100 Hz

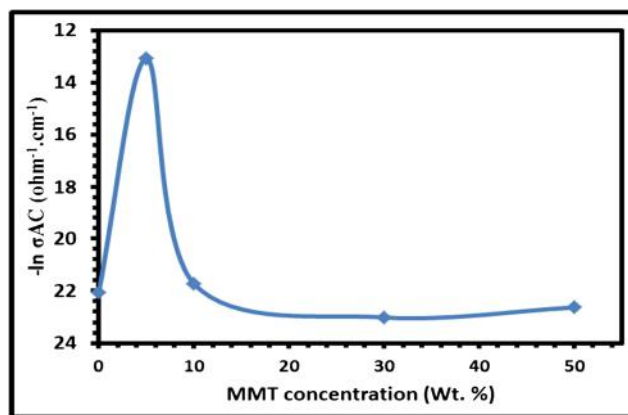


Fig. 9 AC- conductivity values against MMT concentration (wt%) for PMMA-LTF, PMMA-LTF-1, PMMA-LTF-2, PMMA-LTF-3, and PMMA-LTF-4 at room temperature (303 K) and a frequency of 100 Hz

different species in the polymer matrix [41]. Here, it is obvious that the low MMT content of 5 wt% representing the PMMA-LTF-1 sample is the best one in creating those special pathways through the intercalation process, as it exhibited the highest AC- conductivity value at room temperature. Moreover, the activation energy (E_a) values for all investigated samples were also calculated using the Arrhenius model $\sigma = \sigma_0 \exp.(-E_a/RT)$, where R , T , σ , and σ_0 are gas constant, temperature, the AC- conductivity, and the pre-exponential factor, respectively. All activation energy values were shown in Fig. 10. It describes the energy associated with the defect formation and the ion migration simultaneously. Moreover, the value of activation energy basically tells about the favorable environment and the conditions for the ion migration for smoother ion transport. The high value of activation energy may be due to the requirement of high energy for ion migration [42, 43]. In this vein and according to our reported results, the figure showed that the PMMA-LTF-1 sample has the lowest activation energy value ($E_a = 0.65$ eV) compared to the others containing LTF and MMT. This comes in a good

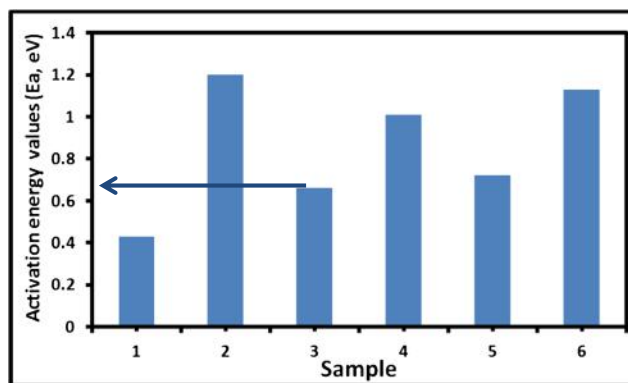


Fig. 10 Activation energy values of 1: PMMA; 2: PMMA-LTF; 3: PMMA-LTF-1; 4: PMMA-LTF-2; 5: PMMA-LTF-3, and 6: PMMA-LTF-4

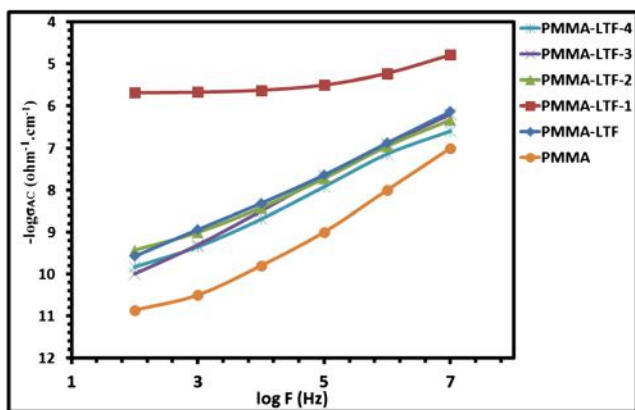


Fig. 11 Frequency dependence of AC- conductivity for PMMA, PMMA-LTF, PMMA-LTF-1, PMMA-LTF-2, PMMA-LTF-3, and PMMA-LTF-4 at room temperature (303 K)

agreement with the highest conductivity value of the same sample. So, ionic conductivity depends on the activation energy of the free ions directly and the smaller the activation energy, the smoother the cation migration. This lowering in the activation energy is owing to the increase of flexibility of polymer chains for this concentration which makes a favorable conductive path for the ions [44]. The other activation energy (E_a) values come as in the following order: (E_a (PMMA) $<$ E_a (PMMA-LTF-3) $<$ E_a (PMMA-LTF-2) $<$ E_a (PMMA-LTF-4) $<$ E_a (PMMA-LTF)).

Figure 11 showed the frequency dependence of AC- conductivity for PMMA, PMMA-LTF, PMMA-LTF-1, PMMA-LTF-2, PMMA-LTF-3, and PMMA-LTF-4 at room temperature (303 K). The figure showed an increase of AC- conductivity values with frequency. Also, the PMMA-LTF-1 sample showed the highest AC- conductivity values compared to all the other ones. According to all the abovementioned results, the PMMA-LTF-1 sample is the best one delivering good conductivity value at room temperature with good thermal

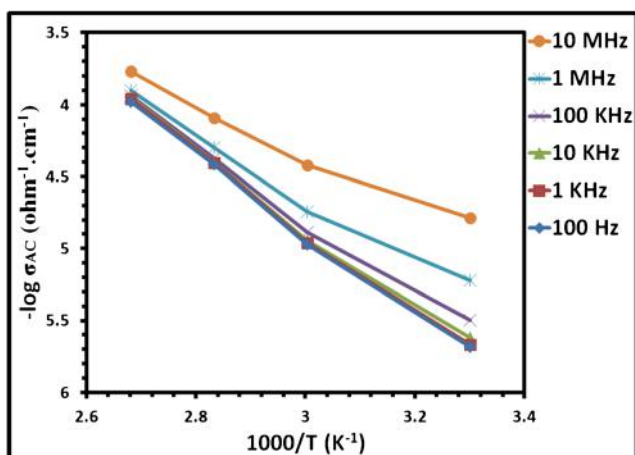


Fig. 12 Temperature dependence of AC- conductivity for PMMA-LTF-1 at different frequencies

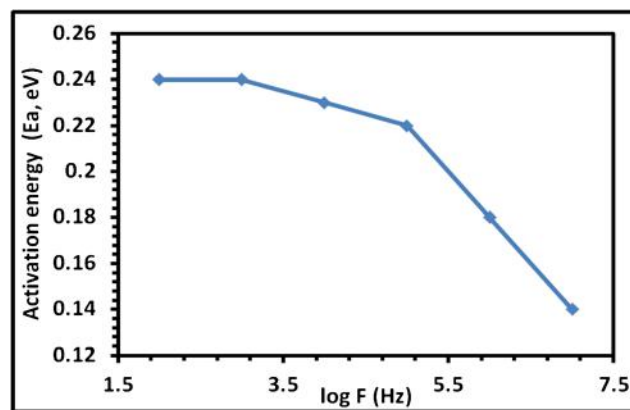


Fig. 13 Frequency dependence of activation energy for PMMA-LTF-1

stability behavior. More studies concerning electrical properties and electrochemical stability will be hereafter discussed to investigate the ability of using this electrolyte membrane as a solid one for the lithium ion batteries application.

Figure 12 represents the temperature dependence of AC- conductivity at different frequencies (100 Hz–10 MHz) for the PMMA-LTF-1 sample. As obviously seen, the AC- conductivity increases with temperature increase, and with frequency increase at the same time. Also, activation energy values at different frequencies were calculated using the abovementioned Arrhenius model. Figure 13 represents the frequency dependence of activation energy for the PMMA-LTF-1 sample. The figure showed a decrease behavior of activation energy values with frequency increase. This can be attributed to the lithium ion mobility enhancement upon frequency increase. Also, the frequency dependence of AC- conductivity at different temperatures for the PMMA-LTF-1 sample were also studied (Fig. 14). The figure showed an increase behavior in two ranges; the first was observed from 0.1 Hz to 100 KHz, and the second was observed from 100 KHz to 20 MHz. Temperature and frequency dependence of dielectric

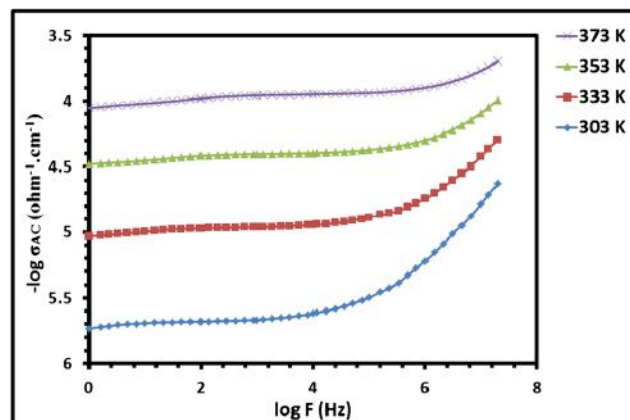


Fig. 14 Frequency dependence of AC- conductivity for PMMA-LTF-1 at different temperatures

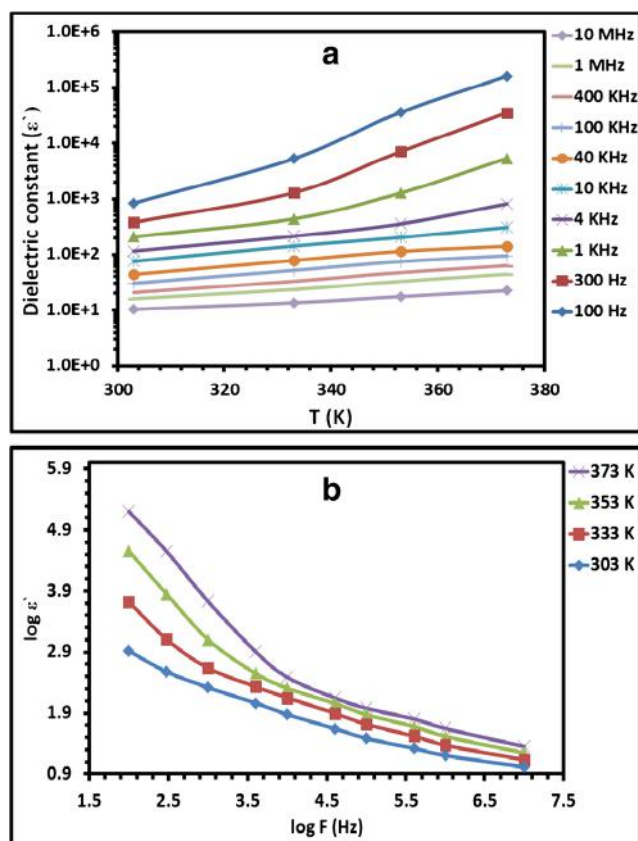


Fig. 15 Dielectric constant versus a temperature, at different frequencies and b frequency, at different temperatures for PMMA-LTF-1

constant at different frequencies (100 Hz to 10 MHz) and temperatures (303 to 373 K), respectively, of PMMA-LTF-1 sample was also investigated, as represented by Fig. 15a, b. Figure 15a showed an increase behavior of dielectric constant with temperature at different frequencies. The increase behavior of dielectric constant with temperature may be attributed to the viscosity decrease [45] of the polymer matrix, and dissolving of the crystalline or semi-crystalline phases in the amorphous phase [46]. Figure 15b showed a decrease behavior of dielectric constant with frequency at different temperatures, which may be attributed to the contribution of charge accumulation at the interface and leads to a net polarization of the ionic medium results in the formation of the space charge region at the electrode–electrolyte interface [47–53]. The PMMA-LTF-1 sample exhibited dielectric constant (ϵ') value equals 834 at room temperature (303 K) and 100 Hz. Figure 16a, b represented the temperature and frequency dependence of dielectric loss at different frequencies (100 Hz to 10 MHz) and temperatures (303 to 373 K), respectively, for PMMA-LTF-1. Figure 16a showed an increase behavior of dielectric loss with temperature at different frequencies. This is due to the relaxation of the dipole molecules in cooperation with the resulting drop in the relaxation time; this in turn exerts a double effect on the dielectric loss, on one hand, the friction between the dipoles will be increased

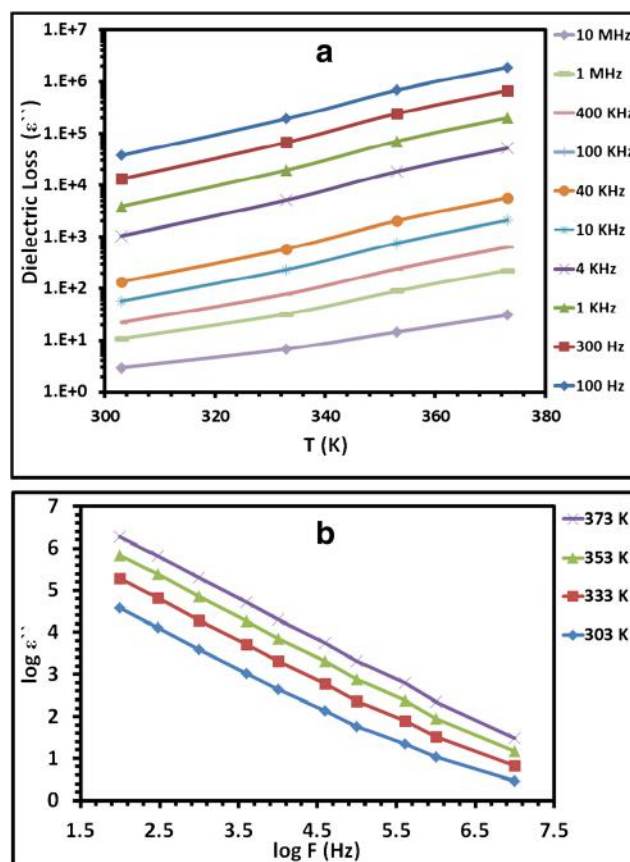


Fig. 16 Dielectric loss versus a temperature, at different frequencies and b frequency, at different temperatures for PMMA-LTF-1

and then the increase in energy dissipation. Figure 16b exhibited a decrease behavior of dielectric loss with frequency at different temperatures. The PMMA-LTF-1 sample showed a value of dielectric loss (ϵ'') equals 37,500 at room temperature (303 K) and 100 Hz.

Figure 17 shows a complex impedance of the PMMA-LTF-1 sample at three different temperatures (303, 333, and 353 K). The figure showed a spectrum consists of a semicircle followed by an inclined straight line. The diameter and height

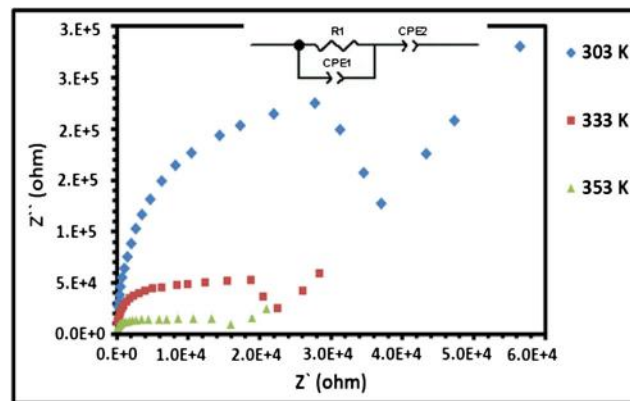


Fig. 17 Complex impedance spectra for PMMA-LTF-1 at different temperatures

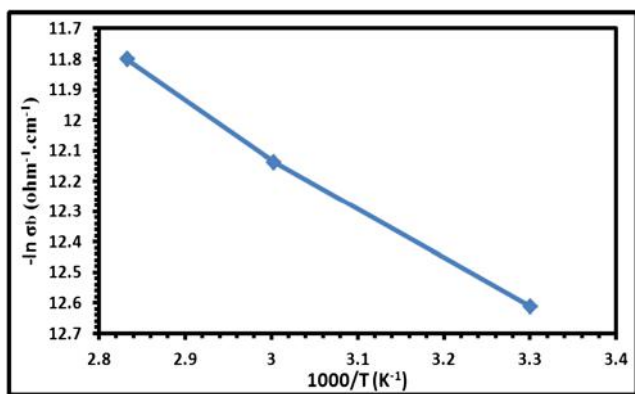


Fig. 18 Temperature dependence of bulk conductivity for PMMA-LTF-1

of the semicircles decrease upon temperature increasing, indicating the impedance decrease with temperature increase. The semicircle part may be attributed to the conduction process, and the linear region one may be due to the effect of the blocking electrode [54–60] that leads to a charge polarization process in the polymer bulk. All bulk ionic conductivity values were calculated at different temperatures. Figure 18 showed the bulk ionic conductivity increase with temperature increasing, exhibiting the following order: ($\sigma_b = 3.33 \times 10^{-6} \Omega^{-1} \cdot \text{cm}^{-1}$ at 303 K)

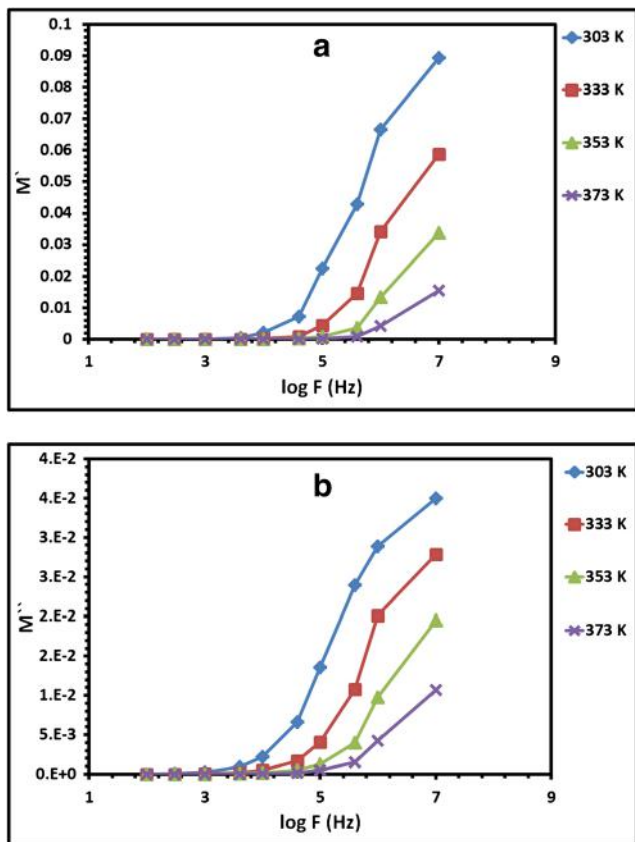


Fig. 19 Frequency dependence of modulus; **a** M' , and **b** M'' at different temperatures for PMMA-LTF-1

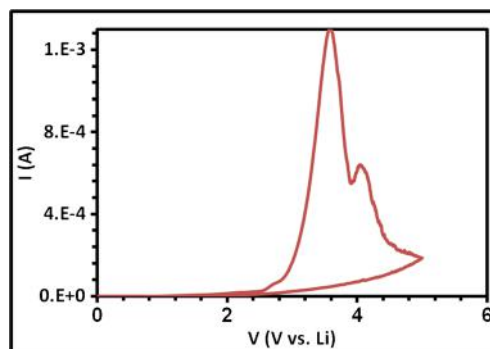


Fig. 20 I-V curve for PMMA-LTF-1 sample at room temperature

$< \sigma_b = 5.36 \times 10^{-6} \Omega^{-1} \cdot \text{cm}^{-1}$ at 333 K) $< \sigma_b = 7.50 \times 10^{-6} \Omega^{-1} \cdot \text{cm}^{-1}$ at 353 K)). Also, the equivalent circuit was determined from the spectrum and shown in Fig. 17. Where R1 is the bulk resistance of the electrolyte, CPE1 is the bulk capacity of the electrolyte and CPE2 is a capacity of bulk electrode–electrolyte interface.

Dielectric modulus was also investigated to study the dielectric relaxation behavior by suppressing electrodes' polarization effect. The real and imaginary parts (M' , M'') of the dielectric modulus for PMMA-LTF-1 sample, at different temperatures, were shown in Fig. 19a, b. In the two figures, the relaxation peaks are absent. Also, abrupt increments were observed in the high-frequency range. In contrast, at the low-frequency range for all temperatures, the sample indicated a long tail prior leading to the zero end. The long tail reveals the suppression of the electrical double layer effect at the contact of the electrode-electrolyte area [61]. According to literatures, the suppression of the electrical double layer is associated with a high capacitance value with the electrode in the polymer electrolyte systems [62].

Figure 20 shows the I-V characteristic curve. The onset voltage for anodic current is determined at around 3 V which is assumed to be the decomposition voltage of the PMMA-LTF-1 sample.

Conclusions

High and low montmorillonite content incorporated polymethylmethacrylate matrix in the presence of lithiumtriflate salt was synthesized using the solution cast technique. All synthesized samples were characterized using different techniques such as XRD, FT-IR, DSC, TG, and SEM. The effect of both LTF salt and MMT filler on the structure of the PMMA matrix was investigated in well sequence. The complete dissolution of LTF salt was observed by XRD analysis. The intercalation of MMT filler within the PMMA matrix was confirmed by XRD through a partially enlarged drawing of the MMT peak (001) in all PMMA-LTF nanocomposites. Also, the interactions between both of LTF

salt and MMT filler with the PMMA matrix were confirmed through the wave number values shifting of the FT-IR analysis. The pure PMMA sample showed the highest value of decomposition temperature ($T_d = 438$ °C) compared to the other ones, which showed the following order: (PMMA-LTF, $T_d = 408$ °C > PMMA-LTF-2, $T_d = 387$ °C > PMMA-LTF-1, $T_d = 378$ °C > PMMA-LTF-4, $T_d = 364$ °C > PMMA-LTF-3, $T_d = 347$ °C). On the other hand, the PMMA-LTF-1 sample (containing only 5 wt% MMT) exhibited the highest AC-conductivity value ($\sigma_{Ac} = 2.09 \times 10^{-6} \Omega^{-1} \cdot \text{cm}^{-1}$, at room temperature) compared to the other ones, which showed the following conductivity order: (σ_{Ac} (PMMA-LTF-2, $3.73 \times 10^{-10} \Omega^{-1} \cdot \text{cm}^{-1}$) > σ_{Ac} (PMMA-LTF, $2.66 \times 10^{-10} \Omega^{-1} \cdot \text{cm}^{-1}$) > σ_{Ac} (PMMA-LTF-4, $1.48 \times 10^{-10} \Omega^{-1} \cdot \text{cm}^{-1}$) > σ_{Ac} (PMMA-LTF-3, $1.01 \times 10^{-10} \Omega^{-1} \cdot \text{cm}^{-1}$) > σ_{Ac} (PMMA, $1.37 \times 10^{-11} \Omega^{-1} \cdot \text{cm}^{-1}$), at room temperature). The PMMA-LTF-1 sample exhibited a dielectric constant and loss values equal to 834 and 37,500, respectively, at room temperature (303 K) and 100 Hz. The electrochemical stability of PMMA-LTF-1 was also investigated through I-V study to show a decomposition voltage of 3 V. At last, the high thermal and electrochemical stability, beside the good ionic conductivity, at room temperature, of the sample (PMMA-LTF-1) containing low content (5 wt%) of MMT make this sample a promising candidate for the lithium ion batteries applications.

Acknowledgments The author (Emad M. Masoud) of this research paper would like to thank the science and technology development fund (STDF), Egypt, (<http://www.stdf.org.eg/index.php/en/>) for the financial support of this scientific research work through Short-Term Fellowship (STF) Project (Project ID: 23173).

References

- Stephan AM, Nahm KS (2006) Review on composite polymer electrolytes for lithium batteries. *Polymer* 47:5952–5964
- Quartarone E, Mustarelli P (2011) Electrolytes for solid-state lithium rechargeable batteries: recent advances and perspectives. *Chem Soc Rev* 40:2525–2540
- Lago N, Garcia-Calvo O, Lopez del Amo JM, Rojo T, Armand M (2015) All-solid-state lithium-ion batteries with grafted ceramic nanoparticles dispersed in solid polymer electrolytes. *ChemSusChem* 8:3039–3043
- Xue Z, He D, Xie X (2015) Poly(ethylene oxide)-based electrolytes for lithium-ion batteries. *J Mater Chem A* 3:19218–19253
- Long L, Wang S, Xiao M, Meng Y (2016) Polymer electrolytes for lithium polymer batteries. *J Mater Chem A* 4:10038–10069
- Yue L, Ma J, Zhang J, Zhao J, Dong S, Liu Z, Cui G, Che L (2016) All solid-state polymer electrolytes for high-performance lithium ion batteries. *Energy Storage Materials* 5:139–164
- Ngai KS, Ramesh S, Ramesh K, Juan JC (2016) A review of polymer electrolytes: fundamental, approaches and applications. *Ionics* 22:1259–1279
- Wang W, Alexandridis P (2016) Composite polymer electrolytes: nanoparticles affect structure and properties. *Polymers* 8(11):387: 1–36
- Choi SW, Kim JR, Ahn YR, Jo SM, Cairns EJ (2007) Characterization of electrospun PVdF fiber-based polymer electrolytes. *Chem Mater* 19:104–115
- Masoud EM (2016) Nano lithium aluminate filler incorporating gel lithium triflate polymer composite: preparation, characterization and application as an electrolyte in lithium ion batteries. *Polym Test* 56:65–73
- Senthil Kumar P, Sakunthala A, Reddy MV, Prabu M (2018) Structural, morphological, electrical and electrochemical study on plasticized PVdF-HFP/PEMA blended polymer electrolyte for lithium polymer battery application. *Solid State Ionics* 319:256–265
- Bohnke O, Frand G, Rezzazi M, Rousselot C, Truche C (1993) Fast ion transport in new lithium electrolytes gelled with PMMA. 1. Influence of polymer concentration. *Solid State Ionics* 66:97–104
- Raghavan P, Manuel J, Zhao X, Kim DS, Ahn JH, Nah C (2011) Preparation and electrochemical characterization of gel polymer electrolyte based on electrospun polyacrylonitrile nonwoven membranes for lithium batteries. *J Power Sources* 196:6742–6749
- Arya A, Sharma AL (2017) Polymer electrolytes for lithium ion batteries: a critical study. *Ionics* 23(3):497–540
- Arya A, Sharma AL (2017) Insights into the use of polyethylene oxide in energy storage/conversion devices: a critical review. *J Phys D Appl Phys* 50(44):443002–443065
- Arya A, Sharma AL (2018) Effect of salt concentration on dielectric properties of Li-ion conducting blend polymer electrolytes. *J Mater Sci Mater Electron* 29(20):17903–17920
- Raghavan P, Zhao X, Shin C, Baek DH, Choi JW, Manuel J, Heo MY, Ahn JH, Nah C (2010) Preparation and electrochemical characterization of polymer electrolytes based on electrospun poly(vinylidene fluoride-co-hexafluoropropylene)/polyacrylonitrile blend/composite membranes for lithium batteries. *J Power Sources* 195:6088–6094
- Sathish S, Shekar BC (2014) Preparation and characterization of nano scale PMMA thin films. *Indian J Pure Appl Phys* 52:64–67
- Noor SAM, Bayley PM, Forsyth M, MacFarlane DR (2013) Ionogels based on ionic liquids as potential highly conductive solid state electrolytes. *Electrochim Acta* 91:219–226
- Carvalho TIS (2013) Development of ion jelly thin films for electrochemical devices. *Faculdade de Ciência e Tecnologia da Universidade Nova de Lisboa*
- Zai-Lai X, Jeličić A, Wang F-P, Rabu P, Friedrich A (2010) Transparent, flexible, and paramagnetic ionogels based on PMMA and the iron-based ionic liquid 1-butyl-3-methylimidazolium tetrachloroferrate(III) [Bmim][FeCl₄]. *J Mater Chem* 20:9543–9549
- Lunstroo K, Driesen K, Nockemann P, Viau L, Mutin PH, Vioux A, Binnemans K (2010) Ionic liquid as plasticizer for europium(III)-doped luminescent poly(methyl methacrylate) films. *Phys Chem Chem Phys* 12:1879–1885
- Masoud EM, Elbellihi A-A, Bayoumy WA, Mousa MA (2013) Organic-inorganic composite polymer electrolyte based on PEO-LiClO₄ and nano-Al₂O₃ filler for lithium polymer batteries: Dielectric and transport properties. *Alloys Compd* 575:223–228
- Zhou J, Fedkiw PS (2004) Ionic conductivity of composite electrolytes based on oligo(ethylene oxide) and fumed oxides. *Solid State Ionics* 166:275–293
- Masoud EM, Hassan ME, Wahdan SE, Elsayed SR, Elsayed SA (2016) Gel P(VdF/HFP)/PVAc/lithium hexafluorophosphate composite electrolyte containing nano ZnO filler for lithium ion batteries application: effect of nano filler concentration on structure, thermal stability and transport properties. *Polym Test* 56:277–286
- Moskwiak M, Giska I, Borkowska R, Zalewska A, Marczewski M, Marczevska H, Wiczorek W (2006) Physico- and electrochemistry of composite electrolytes based on PEODME-LiTFSI with TiO₂. *J Power Sources* 159:443–448
- Sannier L, Zalewska A, Wiczorek W, Marczewski M, Marczevska H (2007) Impact of “Super Acid” like filler on the

- properties of a PEGDME/LiClO₄ system. *Electrochim Acta* 52: 5685–5689
28. Stolarska M, Niedzicki L, Borkowska R, Zalewska A, Wieczorek W (2007) Structure, transport properties and interfacial stability of PVdF/HFP electrolytes containing modified inorganic filler. *Electrochim Acta* 53:1512–1517
 29. Vaia R, Vasudevan S, Krawiec W, Scanlon L, Giannelis E (1995) New polymer electrolyte nanocomposites: melt intercalation of poly(ethylene oxide) in mica-type silicates. *Adv Mater* 7:154–156
 30. Chen H, Chang FC (2001) The novel polymer electrolyte nanocomposite composed of poly(ethylene oxide), lithium triflate and mineral clay. *Polymer* 42:9763–9769
 31. Chen H, Chiu C, Chang F (2002) Conductivity enhancement mechanism of the poly(ethylene oxide)/modified-clay/LiClO₄ systems. *J Polym Sci B Polym Phys* 40:1342–1353
 32. Fan L, Nan C, Dang Z (2002) Effect of modified montmorillonites on the ionic conductivity of (PEO)₁₆LiClO₄ electrolytes. *Electrochim Acta* 47:3541–3544
 33. Chen H, Chang F (2001) Interaction mechanism of a novel polymer electrolyte composed of poly(acrylonitrile), lithium triflate, and mineral clay. *J Polym Sci B Polym Phys* 39:2407–2419
 34. Meneghetti P, Qutubuddin S, Webber A (2004) Synthesis of polymer gel electrolyte with high molecular weight poly(methyl methacrylate)-clay nanocomposite. *Electrochim Acta* 49:4923–4931
 35. Deka M, Kumar A (2010) Enhanced electrical and electrochemical properties of PMMA-clay nanocomposite gel polymer electrolytes. *Electrochim Acta* 55:1836–1842
 36. Aravindan V, Vickraman P (2007) Polyvinylidene fluoride-hexafluoropropylene based nanocomposite polymer electrolytes (NCPE) complexed with LiPF₃(CF₃CF₂)₃. *Eur Polym J* 43: 5121–5127
 37. Saikia D, Chen-Yang YW, Chen YT, Li YK, Lin SI (2008) Investigation of ionic conductivity of composite gel polymer electrolyte membranes based on P(VDF-HFP), LiClO₄ and silica aerogel for lithium ion battery. *Desalination* 234:24–32
 38. Manuel Stephen A, Nahm KS, Kulandainathan MA, Ravi G, Wilson J (2006) Poly(vinylidene fluoride-hexafluoropropylene) (PVdF-HFP) based composite electrolytes for lithium batteries. *Eur Polym J* 42:1728–1734
 39. Duan G, Zhang C, Li A, Yang X, Lu L, Wang X (2008) Preparation and characterization of mesoporous zirconia made by using a poly(methyl methacrylate) template. *Nanoscale Res Lett* 3:118–122
 40. Masoud EM, El-Bellihi A-A, Bayoumy WA, Mohamed EA (2018) Polymer composite containing nano magnesium oxide filler and lithium triflate salt: An efficient polymer electrolyte for lithium ion batteries application. *J Mol Liq* 260C:237–244
 41. Croce F, Appetecchi GB, Persi L, Scrosati B (1998) Nanocomposite polymer electrolytes for lithium batteries. *Nature* 394:456–458
 42. Latif F, Aziz M, Katun N, Yahya MZ (2006) The role and impact of rubber in poly(methyl methacrylate)/lithium triflate electrolyte. *J Power Sources* 159:1401–1404
 43. Mohamad AA, Mohamed NS, Yahya MZ, Othman R, Ramesh S, Alias Y, Arof AK (2003) Ionic conductivity studies of poly(vinyl alcohol) alkaline solid polymer electrolyte and its use in nickel-zinc cells. *Solid State Ionics* 177:156–171
 44. Arya A, Sharma AL (2018) Optimization of salt concentration and explanation of two peak percolation in blend solid polymer nanocomposite films. *J Solid State Electrochem Electrochem* 22:2725–2745
 45. Chodari BVR, Wang W (eds) (2000) *Solid state ionics: materials and devices*. World Scientific, Singapore
 46. Hu L, Tang Z, Zhang Z (2007) New composite polymer electrolyte comprising mesoporous lithium aluminate nanosheets and PEO/LiClO₄. *J Power Sources* 166:226–232
 47. Anderson S, Bohon RL, Kimpton DD (1955) Infrared spectra and atomic arrangement in fused boron oxide and soda borate glasses. *J Am Ceram Soc* 38:370–377
 48. Ren S, Chen Z, Yan T, Han F, Kuang X, Liang F, Liu L (2018) High temperature dielectrics and defect characteristic of (Nb, Mn, Zr) modified 0.4(Ba_{0.8}Ca_{0.2})TiO₃ - 0.6Bi(Mg_{0.5}Ti_{0.5})O₃ ceramics. *J Phys Chem Solids* 118:99–108
 49. Han F, Ren S, Deng J, Yan T, Ma X, Peng B, Liu L (2017) Dielectric response mechanism and suppressing high-frequency dielectric loss in Y₂O₃ grafted CaCu₃Ti₄O₁₂ ceramics. *J Mater Sci Mater Electron* 28:17378–17387
 50. Deng J, Liu L, Sun X, Liu S, Yan T, Fang L, Elouadi B (2017) Dielectric relaxation behavior and mechanism of Y_{2/3} Cu₃ Ti₄ O₁₂ ceramic. *Mater Res Bull* 88:320–329
 51. Han F, Deng J, Liu X, Yan T, Ren S, Ma X, Liu S, Peng B, Liu L (2017) High-temperature dielectric and relaxation behavior of Yb-doped Bi_{0.5}Na_{0.5}TiO₃ ceramics. *Ceram Int* 43:5564–5573
 52. Sun X, Deng J, Liu S, Yan T, Peng B, Jia W, Mei Z, Hongbo S, Fang L, Liu L (2016) Grain boundary defect compensation in Ti-doped BaFe_{0.5}Nb_{0.5}O₃ ceramics. *Appl Phys A* 122(864):1–8
 53. Liu S, Sun X, Peng B, Su H, Mei Z, Huang Y, Deng J, Su C, Fang L, Liu L (2016) Dielectric properties and defect mechanisms of (1-x)Ba(Fe_{0.5}Nb_{0.5})O₃-xBiYbO₃ ceramics. *J Electroceram* 37:137–144
 54. Masoud EM, El-Bellihi A-A, Bayoumy WA, Mousa MA (2013) Effect of LiAlO₂ nanoparticle filler concentration on the electrical properties of PEO-LiClO₄ composite. *Mater Res Bull* 48(3):1148–1154
 55. ElBellihi AA, Bayoumy WA, Masoud EM, Mousa MA (2012) Preparation, Characterizations and Conductivity of Composite Polymer Electrolytes Based on PEO-LiClO₄ and Nano ZnO Filler. *Bull Korean Soc* 33(9):2949–2954
 56. Masoud EM, Khairy M, Mousa MA (2013) Electrical properties of fast ion conducting silver based borate glasses: application in solid battery. *Alloys Compd* 569:150–155
 57. Masoud EM, Mousa MA (2015) Silver-doped silver vanadate glass composite electrolyte: structure and an investigation of electrical properties. *Ionics* 21:1095–1103
 58. Masoud EM (2015) Citrated porous gel copolymer electrolyte composite for lithium ion batteries application: An investigation of ionic conduction in an optimized crystalline and porous structure. *Alloys and compounds* 651:157–163
 59. Prasad Rao R, Reddy MV, Adams S, Chowdari BVR (2012) Preparation and mobile ion transport studies of Ta and Nb doped Li₆Zr₂O₇ Li-fast ion conductors. *Mater Sci Eng B* 177:100–105
 60. Reddy MV, Adams S (2017) Molten salt synthesis and characterization of fast ion conductor Li_{6.75}La₃Zr_{1.75}Ta_{0.25}O₁₂. *J Solid State Electrochem* 21:2921–2928
 61. Shastry MCR, Rao KJ (1991) ac conductivity and dielectric relaxation studies in AgI-based fast ion conducting glasses. *Solid State Ionics* 44:187–198
 62. Suthanthiraraj SA, Sheeba DJ, Paul BJ (2009) Impact of ethylene carbonate on ion transport characteristics of PVdF-AgCF₃SO₃ polymer electrolyte system. *Mater Res Bull* 44:1534–1539